ChemSusChem

Research Article
doi.org/10.1002/cssc.202202019

Chemistry Europe
European Chemical Societies Publishing

www.chemsuschem.org

A Dual Fluorescence Assay Enables High-Throughput Screening for Poly(ethylene terephthalate) Hydrolases

Kun Liu,[a] Ziping Xu,[a] Zhiyi Zhao,[a] Yuexing Chen,[a] Yating Chai,[a] Li Ma,[a] and Shengying Li*[a, b]

The drastically increasing consumption of petroleum-derived plastics hasserious environmental impacts and raises public concerns. Poly(ethylene terephthalate) (PET) is amongst the most extensively produced synthetic polymers. Enzymatic hydrolysis of PET recently emerged as an enticing path for plastic degradation and recycling. In-lab directed evolution has revealed the great potential of PET hydrolases (PETases). However, the time-consuming and laborious PETase assays hinder the identification of effective variants in large mutant libraries. Herein, we devise and validate a dual fluorescence-based high-throughput screening (HTS) assay for a representative *Is*PETase. The two-round HTS of a pilot library consisting of 2850 *Is*PETase variants yields six mutant *Is*PETases with 1.3–4.9 folds improved activities. Compared to the currently used structure- or computational redesign-based PETase engineering, this HTS approach provides a new strategy for discovery of new beneficial mutation patterns of PETases.

Introduction

Synthetic plastics have pervaded almost every aspect of modern human life due to low cost, light weight and desirable properties such as durability, plasticity and transparency.[1] However, tremendous consumption and "poorly reversible" emission of plastics have led to serious environmental pollution and growing public concerns owing to the considerably low rate of natural degradation and recycling.[2] Therefore, it is widely recognized that global action is urgently required to reduce plastic production and consumption, as well as promote sustainable handling of plastics, such as reusage, recycling, and value chain revolution. Despite chemical and thermochemical approaches, biotechnological processes have also been considered a promising solution for plastic waste degradation and recycling.[3,4]

Poly(ethylene terephthalate) (PET) is the most abundantly consumed polyester[5] and accounts for 12% by volume of the global solid waste.[6] Meanwhile, PET hydrolytic enzymes (PHEs) have continuously been reported during the last two decades.[7,8] In 2016, a cutinase-like PHE termed *Is*PETase was identified from a PET-assimilating bacterial strain *Ideonella sakaiensis* 201-F6.[9] Amongst the reported PHEs, *Is*PETase exhibited superior activity at ambient temperature, generating terephthalic acid (TPA), ethylene glycol (EG), mono(2-hydroxyethyl) terephthalic acid (MHET) and bis(2-hydroxyethyl) terephthalic acid (BHET) as products. Subsequently, the catalytic mechanism of *Is*PETase was analyzed biochemically and structurally.[10–13]

Bearing functional novelty and application potential, rational design and directed evolution approaches for PET hydrolases have been conducted for higher performance and robustness. Numerous *Is*PETase variants with diverse single-point mutations resulted in 1.2–3.1 folds higher PET hydrolytic activities.[10,11,14,15] Furthermore, structure- or computational redesign-based engineering gave rise to outperformed mutant variants, including *Is*PETase$^{S121E/D186H/R280A}$,[16] DuraPETase[17] and FAST-PETase.[18] Meanwhile, engineering of a thermophilic PHE, termed LCC,[19] resulted in variants with elevated thermostability and PET depolymerization activity.[20,21] More importantly, both *Is*PETase and LCC variants have provided a prospective concept of closed PET recycling loop,[18,21] paving a sustainable and innovative path to the future of plastics. Hence, extruding the enzymes' fullest limit will not only tackle the challenge of PET decomposition efficiency, but also benefit the competition of PET upcycling with petroleum-derived virgin materials. However, the paucity of effective strategies and methodologies for high-throughput activity assessment hinders high-efficient laboratorial evolution of PHEs. To address this issue, various analytical methods have been developed for determination of PET hydrolysis products, including spectrographic or titrimetric measurements, and Fenton reaction based fluorimetric assays.[22] Nevertheless, accurate screening requires concentration determination for both enzymes and reaction products in order to evaluate specific enzyme activities. During recent directed evolution of PHEs, tens to hundreds of mutant variants had to be purified[11,16–18,20,23] or semi-purified,[21] followed by product quantification using high-performance liquid chromatography (HPLC). Withstanding discontinuous and time-consuming assays, "compromised" rather than "rational" designs were

[a] Dr. K. Liu, Z. Xu, Z. Zhao, Y. Chen, Y. Chai, Dr. L. Ma, Prof. Dr. S. Li
State Key Laboratory of Microbial Technology
Shandong University
No. 72 Binhai Road, Qingdao, Shandong 266237 (P. R. China)
E-mail: lishengying@sdu.edu.cn
[b] Prof. Dr. S. Li
Laboratory for Marine Biology and Biotechnology
Qingdao National Laboratory for Marine Science and Technology
No. 168 Wenhai Middle Rd, Qingdao, Shandong 266237 (P. R. China)

Supporting information for this article is available on the WWW under https://doi.org/10.1002/cssc.202202019

conceivably endured during the superb mutants hunting of PHEs.

Identification of significantly improved but rare enzyme variants from large-to-huge libraries is the major challenge for directed evolution approaches. Thus, it is urgent to develop high-throughput screening (HTS) methods to facilitate the PHE engineering. Fluorescence-based read-outs are considered as golden standard for HTS.[24] A promising conceptual approach for PHE screening is the application of fluorogenic probes (FPs), which are nonfluorescent and only become fluorescent upon hydrolysis of the intramolecular ester bonds.[25] Fluorescein dibenzoate was used as PET modelling FP in a droplet sorting method, through which PET-degrading microbial species were successfully isolated from the wastewater of a PET textile mill.[26] Another probe fluorescein dilaurate (FDL) was embedded into a set of aliphatic polyesters, and the esterase catalyzed co-hydrolysis of FDL to fluorescein accomplished a fluorescent indication of aliphatic polyester depolymerization.[27] Regarding the convenient enzyme quantification, fluorescent protein labeling renders target protein fluorescently detectable, and more importantly, with fixed stoichiometry.[28] When fused to a cyan fluorescent protein, mutant variants of *Is*PETase were fluorescently normalized for preliminary activity screening.[15] Despite the currently available PHE analysis approaches as described above, there is still no appropriate HTS method for rapid identification of activity improved variants from a large PHE mutant library.

In this study, we developed a dual fluorescence-based HTS approach for *Is*PETase on a 96-well plate basis, enabling rapid determination of enzyme concentration and PET hydrolysis products through rapid plate reading. This approach was then applied for screening a random mutant library of *Is*PETase, and resulted in a small scale of candidates for further enzyme activity determination. Finally, mutant variants were efficiently obtained with 1.3–4.9 folds of improved PET hydrolytic activity. This HTS approach provides a new strategy for discovery of beneficial mutations in *Is*PETase as well as other PHEs, and will prospectively provide new mutation selections for the future PHE engineering.

Results and Discussion

Design of the dual fluorescence-based *Is*PETase assay

To develop a screening strategy on a 96-well plate basis, the main challenge lies in the rapid and continuous determination of product/enzyme concentrations by direct plate reading. The designed approach for HTS of *Is*PETase mutant variants is schematically shown in Figure 1. Briefly, *Is*PETase variants are labeled by fusion of a deep red fluorescent protein to facilitate the direct quantitative determination of enzyme concentrations in a black 96-well plate (plate 1). Meanwhile, a specific 96-well plate is prepared by coating mixed PET-FP on bottoms of each well of plate 2, which followed the previously reported approach for aliphatic polyesters,[27] with appropriate adaptions and modifications on the solvent and evaporation temperature. After transferring appropriate amount of crude

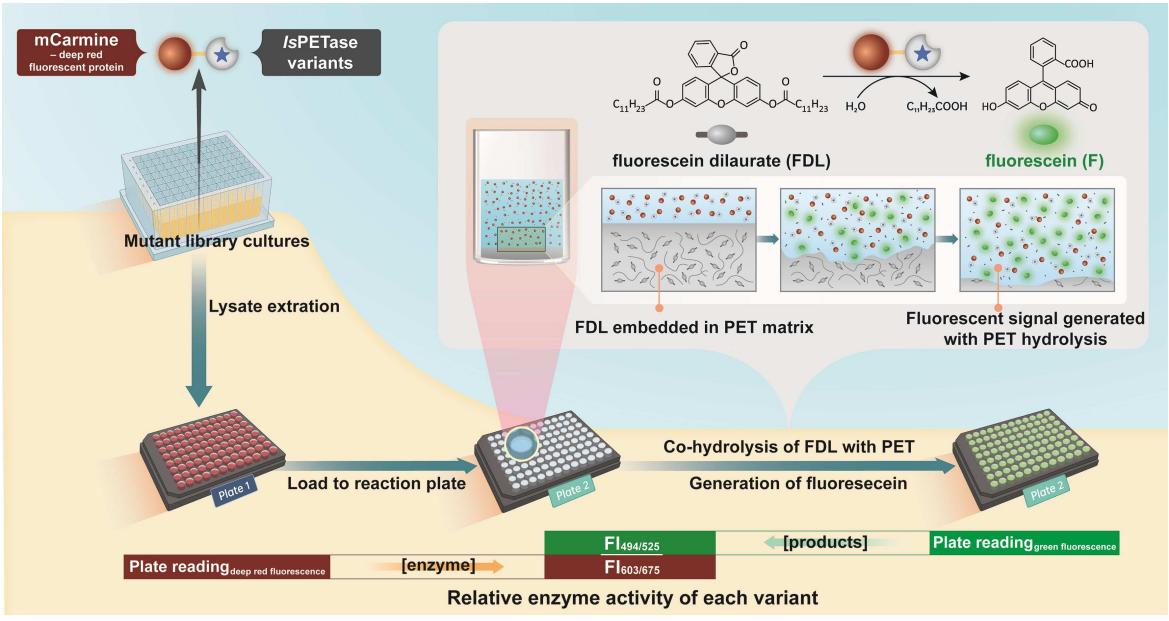

Figure 1. Schematic design for high-throughput screening of *Is*PETase variants. *Is*PETase variants are expressed in 96-deepwell plates as fusion proteins in frame with a deep red fluorescent protein mCarmine. The extracted clear cell lysates are transferred into plate 1 for deep red FI (excitation/emission wavelength: 603/675 nm) detection for enzyme normalization. In each well of prepared plate 2, PET-FDL films are coated on the bottoms as substrates. The PET hydrolysis reactions are initiated by transferring appropriate amounts of cell lysates from plate 1 to plate 2. Simultaneous release and co-hydrolysis of FDL occur during the hydrolytic disruption of PET matrix by *Is*PETase, generating green fluorogenic F, which was previously described in applying FDL embedded aliphatic polyesters.[27] After a period of reaction, the green FI (excitation/emission wavelength: 494/525 nm) in each well is recorded as indication of the reaction products. Finally, the relative enzyme activity of *Is*PETase variants is acquired as the calculated ratio of $FI_{494/525}/FI_{603/675}$.

cell lysate from plate 1 to plate 2, depolymerization of PET occurs accompanied by rapid co-hydrolysis of freed FP to fluorescein. The PET hydrolysis is then quantified by green fluorescence intensity at the end of reaction. Thus, the relative activity of variants in each well can be determined by the ratio calculation of two fluorescent intensity (FI) values. Herein, we used a previously engineered variant *Is*PETase$^{S121E/D186H/R280A}$ (designated P^{EHA})[16] for method validation, and the wild type *Is*PETase as a template for random mutant library construction and screening (Figure S1).

Evaluation of FPs embedding affinity and homogeneity in PET matrix

In-lab preparation of plastic films could be conveniently conducted by dissolving plastic granules in proper organic solvent and evaporating on glass dishes.[17,29] Moreover, embedding FP in the aliphatic polyester matrix was achieved by addition of appropriate amount of FP to the polymer solutions.[27] However, to the best of our knowledge, there is no reported preparation or application of PET-FP films for enzymatic assays. Thus, we initiated this study by preparing PET-FP films with amorphous GfPET (ES301445, Goodfellow, Huntingdon, England), which was commonly used as substrate to determine PET hydrolysis activity in previous reports.[13,18,21] Three commercially available FPs were selected, including fluorescein (F), fluorescein diacetate (FDA) and fluorescein dilaurate (FDL). The binding affinity of FPs embedded in PET matrix was determined by testing the spontaneous fluorescence leaking when PET-FP films were incubated with *Is*PETase reaction buffer. Among PET-F, PET-FDA and PET-FDL, PET-FDL exhibited extremely low spontaneous fluorescence leaking, giving the $FI_{494/525}$ values under 5 at 30, 40 or 50 °C; and this value slightly increased to 26 at 70 °C (Figure 2a). Comparatively, F and FDA were more easily to be spontaneously released from PET matrix, exhibiting the temperature-related growing $FI_{494/525}$ values of 26–104 between 30–50 °C and very high values to 2150 for PET-F and 4000 for PET-FDA at 70 °C. Of note, FDA and FDL should be nonfluorescent because of their diester form, but readily hydrolyzed to fluorogenic F by esterases and lipases.[25,27] Thus, the unexpected $FI_{494/525}$ values of PET-FDL and PET-FDA in absence of P^{EHA} were likely resulted from the spontaneous hydrolysis of FDL or FDA in glycine–NaOH buffer (pH 9.0) at 30–70 °C. Supporting this, addition of 50 nM of P^{EHA} to the ending point solutions and incubation for additional 24 h resulted in no significant change of $FI_{494/525}$ values (Figure 2a). Despite the observation of the spontaneous ester hydrolysis, we confirmed that the P^{EHA}-catalyzed FDL hydrolysis was much faster than the non-enzymatic hydrolysis. Specifically, when PET matrix-free FDL was incubated with P^{EHA}, the $FI_{494/525}$ increasing rate was 8–12 folds as high as that under the buffer only condition (Figure S2). Taken together, these results suggested that the

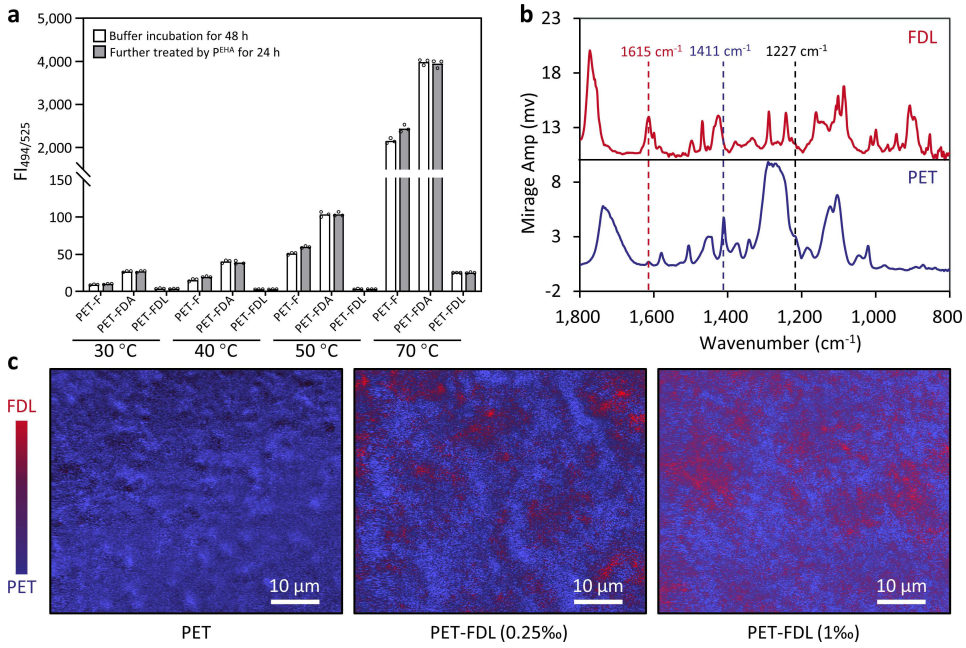

Figure 2. Binding affinity and distribution homogeneity of FPs in PET matrix. a) fluorescence leaking of F, FDA and FDL from PET matrix. PET-F, PET-FDA and PET-FDL films with a respective FP content of 1 ‰ (*w*/*w*) were incubated with 200 μL of glycine–NaOH buffer (pH 9.0) at 30, 40, 50 and 70 °C. After 48 h of incubation in 96-well plates, 150 μL of supernatants were transferred to a new plate for green FI determination (excitation/emission wavelength: 494/525 nm). $FI_{494/525}$ of the transferred sample was recorded again after further treatment with 50 nM of P^{EHA}. All assays were performed in triplicate and the circles represent the individual values. b) O-PTIR spectra of FDL and PET. The spectra were collected within a wavenumber range of 800–1800 cm^{-1}. The wavelengths for generating ratio maps are indicated inside as dotted lines. c) Ratio maps of PET and PET-FDL films. The data were collected in regions of 60×50 μm^2, 5 μm under the surface of PET and PET-FDL films. The ratio maps were generated by dividing the images acquired at 1615 cm^{-1} and 1411 cm^{-1} by 1227 cm^{-1}. The O-PTIR data were collected on mIRage Infrared Microscope and ratio maps were produced using PTIR Studio software (v.4.3.7471, Photothermal Spectroscopy Corp., Santa Barbara, USA).

long aliphatic chain of laurate might benefit the binding affinity of FDL with PET matrix, thereby rapidly providing fluorescent signal with negligible noise during the PET hydrolysis reaction. The performance of FDL for embedding was also reported to be superior comparing to FDA when applied in a series of aliphatic polyesters.[27]

To be used as an indicator of PET hydrolysis, FDL should also be homogeneously distributed in PET matrix to produce stoichiometric fluorescence during PET hydrolysis. Thus, we evaluated FDL distribution by optical photothermal infrared (O-PTIR) microspectroscopy, which is a newly emerging technique and has been used for super resolution imaging of plastic materials[30] and protein aggregations.[31] As a result, the O-PTIR spectra (1800–800 cm^{-1}) of FDL and PET displayed distinct peaks at 1411 cm^{-1} and 1615 cm^{-1}, respectively (Figure 2b). The intensity value at 1227 cm^{-1} was applied as reference to generate the ratio maps (Figure 2c), which demonstrated fine homogeneity of FDL in PET matrix.

Correlation between fluorescence release and PET hydrolysis

Based on the binding affinity and homogeneous distribution of FDL embedded in PET, we reasoned that the proportional amount of FDL would release with the *Is*PETase-catalyzed PET hydrolysis. Subsequently, fluorescein would accumulate simultaneously through enzymatic and non-enzymatic co-hydrolysis of FDL, thus providing the fluorescent signal correlated with PET hydrolysis products. To validate this, $FI_{494/525}$ values were recorded continuously during P^{EHA} catalyzed PET-FDL hydrolysis. Under different temperatures and FDL loadings, the $FI_{494/525}$ values unanimously increased during the 48 h reactions and fit typical enzymatic product concentrations against time curves (Figure 3a–c). Of note, the normalized FI values at each time point exhibited distinct ratios comparing to the theoretical values, which were 1:0.5:0.33:0.25 according to the FDL doping ratios in PET (left bottom of Figure 3a). This phenomenon could be explained by the two reasons: 1) The dynamics of F in solution might be in equilibrium between an "open" fluorescent quinoid form and a "closed" nonfluorescent lactone;[25] and 2) Fluorescein monolaurate was generated as an intermediate exhibiting weak fluorescence, which was previously described[27] (Figure S3). Consequently, the normal-

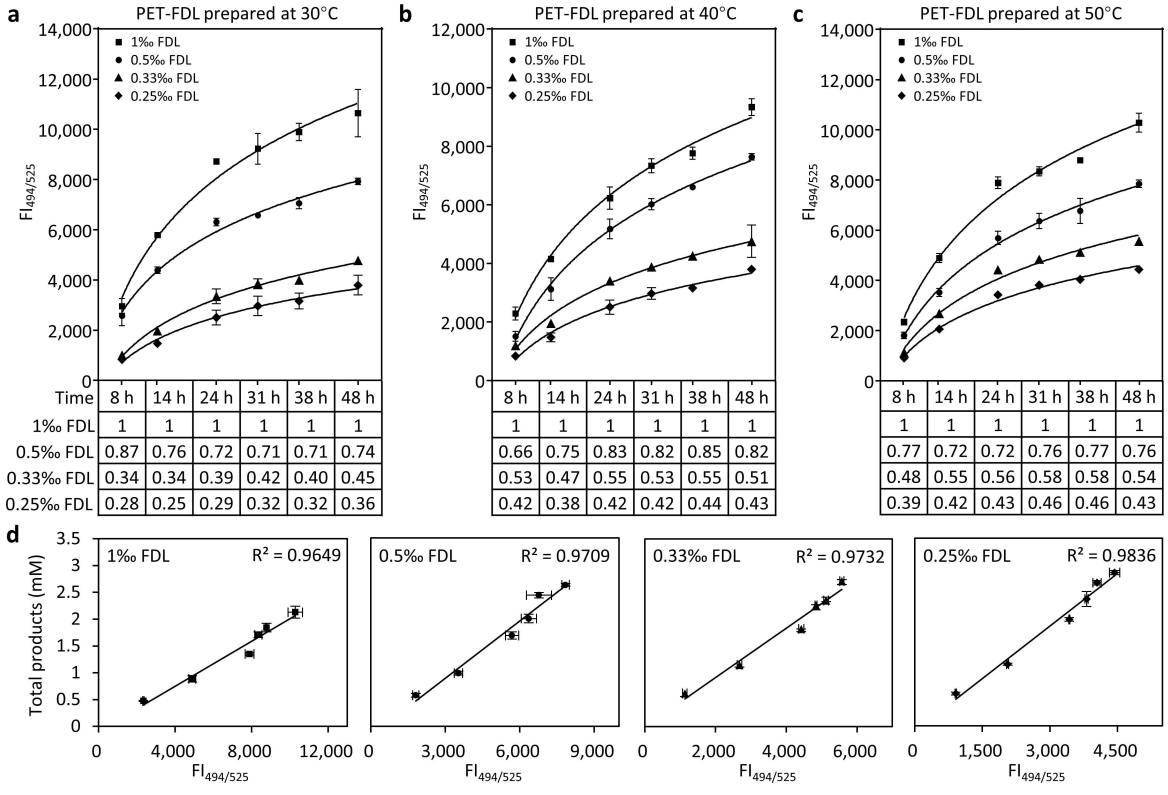

Figure 3. Fluorescence generation and correlation with PET hydrolysis. a–c) Time courses of fluorescence generated during the P^{EHA} catalyzed hydrolysis of PET films embedded with 1‰ (square), 0.5‰ (circle), 0.33‰ (triangle) and 0.25‰ (diamond) of FDL (*w*/*w*). PET-FDL films were prepared by solvent-cast into polypropylene black 96-well plate and evaporating at 30 °C (a), 40 °C (b), and 50 °C (c). The normalized FI values for each time point are shown in the tables below, with different FDL doping ratios indicated on the left bottom of (a). d) Linear correlations of total PET hydrolysis products with $FI_{494/525}$ values in (c). The symbols indicating different FDL content in PET matrix are the same as described above. The total products consist of three PET hydrolysis products including TPA, MHET and BHET, which were quantified by HPLC analysis. The straight lines exhibit linear regression for each kind of PET-FDL films and the R square values are indicated in each box. Triplicated determination of FI values and the corresponding total products were performed and data is shown as means ± standard deviations.

ized FI intensities were higher than theoretical values when lower FDL doping ratios were applied in PET (bottom tables of Figure 3a–c). Nonetheless, this was not an issue for the quantitative indication of PET hydrolysis using $FI_{494/525}$ values. In addition to the spontaneous hydrolysis of FDL as described above (Figure 2a), P^{EHA} catalyzed PET matrix-free FDL hydrolysis to generate fluorescence in a rate of 97.6 $FI_{494/525}\,h^{-1}\,nM_{Enzyme}{}^{-1}$ within 0.5 h, (Figure S2), which was 16-fold higher than the rate when the same amount of FDL was embedded in PET (5.9 $FI_{494/525}\,h^{-1}\,nM_{Enzyme}{}^{-1}$) during the initial 8 h (Figure 3c). Thus, the steady-state of fluorescence dynamics is supposed to form rapidly along with PET hydrolysis. More importantly, the confidence linear regression fitting (Figure 3d, $R^2 > 0.96$) exhibited strong correlation between PET hydrolysis products and $FI_{494/525}$ values (Figure 3c). Additionally, when PET-FDL (1‰) films were hydrolyzed by different amounts (20–500 nM) of P^{EHA}, the total products of PET hydrolysis also showed linear correlation with $FI_{494/525}$ values (Figure S4). Thus, we concluded that $FI_{494/525}$ values should be able to accurately and continuously indicate the reaction process of PET hydrolysis in a dynamic range of enzyme concentrations. Considering the time saving of evaporation at higher temperature and more sensitive signal release with higher FDL content, preparation of PET-FDL (1‰) evaporating at 50 °C was chosen in the following experiments.

Fluorescent protein labeling of *Is*PETase for enzyme quantification

For enzymes naturally exhibiting visible colors, for example, cytochrome P450 enzymes, the amount of target proteins in different cell lysates is conveniently readable.[32] However, when expression of a large mutant library was conducted in 96-deepwell plates, colorless *Is*PETase is unable to be distinguished from other constitutively expressed proteins of the host strain. Fluorescent protein labeling has been widely used for protein subcellular localization[33] and quantitative enzyme normalization.[15,34] Thus, for rapid quantification in 96-(deep)well plate, we sought to express *Is*PETase variants as fusion proteins with a fluorescent tag. We explored FPbase (https://www.fpbase.org/) for an appropriate fluorescent protein with the following characteristics: 1) the excitation and emission wavelengths are distinguished from fluorescein to avoid crosstalk during the green fluorescent reading; 2) it should be a natural monomeric protein to avoid protein aggression when fused with *Is*PETase; and 3) no cofactor is required during the fluorescence emission. Thus, a deep red fluorescent protein mCarmine (FPbase ID: LG377) with the excitation/emission wavelengths at 603/675 nm was selected, which is an eqFP578 mutant variant originated from *Entacmaea quadricolor*.[35]

To examine whether mCarmine exhibits a crosstalk effect with green fluorescence detection, the FIs of purified mCarmine in a series concentrations were determined at 494/525 nm. When mCarmine was within 2 μM, the $FI_{494/525}$ values were less than 20 (Figure S5a), being negligible comparing to $FI_{494/525}$ values generated during PET-FDL hydrolysis reactions (Figure 3a–c). mCarmine was then fused to *N*- or *C*-terminus of P^{EHA}, linked with an empirical flexible or rigid linker,[36] yielding four versions of fusion proteins including P^{EHA}-r-C, P^{EHA}-f-C, C-r-P^{EHA} and C-f-P^{EHA} (Figure S1). The $FI_{603/675}$ values and PET hydrolysis activities of the fusion proteins were subsequently evaluated. Based on comparison of the slopes of linear regression fittings indicating the fluorescence strength of each fused protein and mCarmine (Figure S5b), C-r-P^{EHA} and C-f-P^{EHA} exhibited higher fluorescence strength than P^{EHA}-r-C and P^{EHA}-f-C. Moreover, C-r-P^{EHA} and C-f-P^{EHA} showed higher hydrolytic activities, which were 2–3 folds as high as P^{EHA}-r-C and P^{EHA}-f-C, and even 1.9-fold as high as P^{EHA} without the fluorescence tag (Figure S5c). It was reported that comparing to *Is*PETase, a 3–5 folds higher activity was achieved when MHETase was fused to the *N*-terminus of *Is*PETase, whereas no expression was achieved with *C*-terminus fusion.[37] Meanwhile, a number of hydrophobic peptide tags were found to behave as anchors and enhanced the binding affinities and activities toward PET.[38] Coincidentally, fluorescent proteins, including Neptune[39] from which mCarmine was derived, are typically constituted with highly hydrophobic 11 β-sheets barrel structures. Thus, we deduced that the additional binding affinity conferred by mCarmine might be responsible for the activity enhancement of C-r-P^{EHA} or C-f-P^{EHA}. Considering the rigid linker would keep a fixed distance between the fused domains and maintain their independent functions,[36] C-r-P^{EHA} was applied to evaluate and validate the following HTS assays, whereas the wild type *Is*PETase fused construct C-r-P^{WT} was used for construction of the random mutant library (Figure S1 in the Supporting Information).

Screening of an IsPETase random mutant library

Based on the results of PET-FDL co-hydrolysis and fluorescent protein labeling, $FI_{494/525}/FI_{603/675}$ was used to indicate the relative activity during the HTS process (Figure 1). The designed HTS approach was first evaluated by Z′ factor, which is a screening window coefficient widely used for assay quality assessment, especially for HTS assays.[40] A measurement of separation between positive (C-r-P^{EHA}) and negative (mCarmine) controls was conducted, with the detailed experimental and calculation procedures described in the Supporting Information. The Z′ factor value was calculated to be 0.77 based on the data collected (Figure S6), indicative of an excellent assay.[40]

Subsequently, the HTS method was applied to screen a random mutant library constructed by error-prone PCR. A total of 2850 mutant variants with an average of 1–7 amino acid substitutions were screened, with a C-r-P^{WT} sample as control on each plate. The summarized heat map (Figure 4a) was generated from normalized $FI_{494/525}/FI_{603/675}$ divided by the average value of C-r-P^{WT}. It was noticed that during the Z′ factor evaluation, the $FI_{494/525}/FI_{603/675}$ values fluctuated between 95–161 (Figure S6), exhibiting approximate two-fold

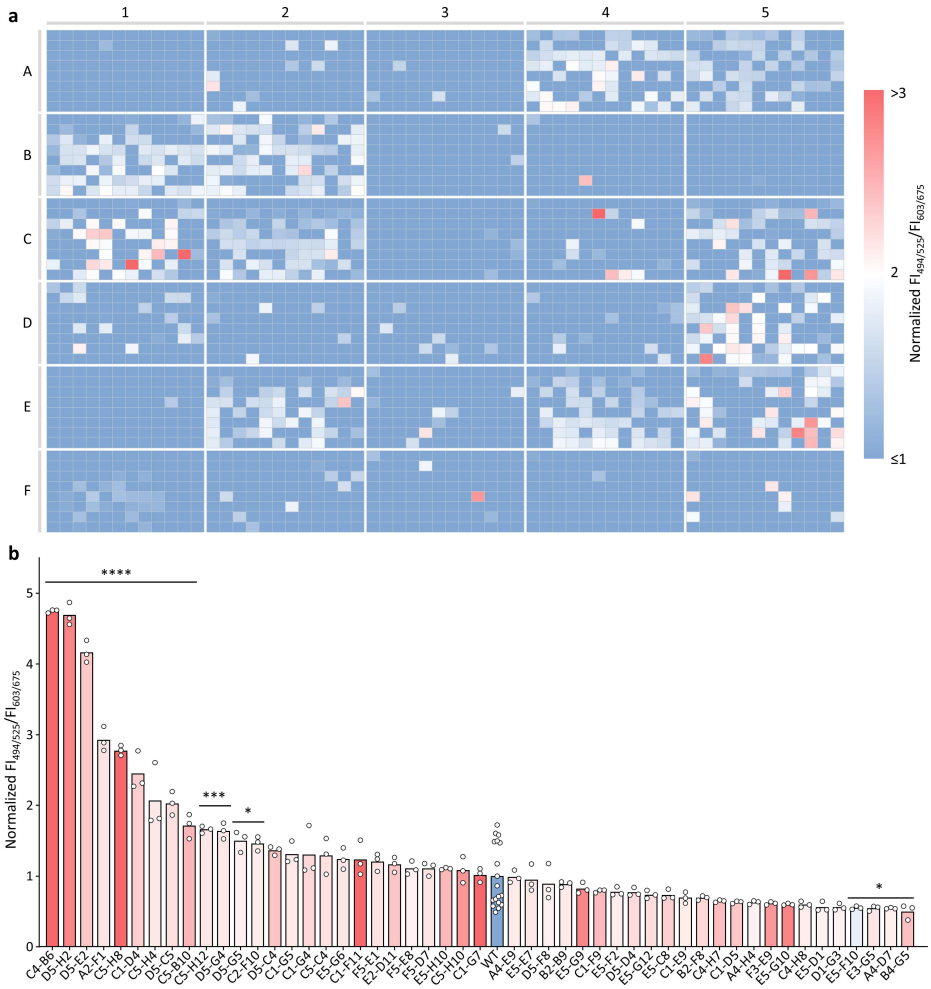

Figure 4. HTS results of an *Is*PETase random mutant library. a) A total number of 2850 *Is*PETase mutant variants were screened on 30 pieces of 96-well plates with a wild type (WT) sample on each plate. The 96-deepwell plate cultured cells were disrupted and the $FI_{603/675}$ values of clear cell lysates were recorded (in plate 1) before transferring to plate 2. After 24 h incubation at 40 °C, $FI_{494/525}$ values were determined and subsequently the $FI_{494/525}/FI_{603/675}$ values were calculated. The basic threshold for the heat map was set as 1 normalized by the mean value of WT samples. The color indicated values by the heat map exhibit the relative activity of each variant. b, Rescreening of the top 50 variants from the screening results of random mutant library. Triplicated experiments were conducted for each individual variant and 18 replicates for C-r-P^{WT}. The bars and circles represent the average and individual normalized $FI_{494/525}/FI_{603/675}$ values divided by the mean value of C-r-P^{WT}. The colors of the bars exhibit the original values depicted in (a). Statistical analyses using a one-way ANOVA multiple comparation were performed to compare the variants and WT. *$P < 0.05$, ***$P < 0.001$, ****$P < 0.0001$.

Table 1. Verification of selected mutant variants screened from the *Is*PETase random mutant library.

Mutant variants	Amino acid substitution	Relative $FI_{494/525}/FI_{603/675}$ in the 1st screening	Relative $FI_{494/525}/FI_{603/675}$ in the 2nd screening	Relative activity
WT	–	1	1	1
C4-B6	V52I A209T S223T	3.6	4.7	1.6
D5-H2	D220N	3.0	4.7	2.5
D5-E2	F106S	2.5	4.2	0.99
A2-F1	S242T	2.3	2.9	4.9
C5-H8	V107I	4.6	2.8	1.6
C1-D4	R260H	2.5	2.5	1.3
C5-H4	A226V	2.3	2.1	2.9
C5-H12	T151I	2.3	1.7	1.3

variation for a fixed mutant variant. Therefore, 50 mutant variants with the highest normalized $FI_{494/525}/FI_{603/675}$ values, distributed from 2.2 to 4.6 in Figure 4a, were selected for a second round of screening in a triplicate setup. Considering the value fluctuation, 18 replicated samples in randomly selected wells were assessed for C-r-P^{WT}. As shown in Figure 4b, 13 mutant variants significantly exhibited higher relative $FI_{494/525}/FI_{603/675}$ values comparing to C-r-P^{WT} based on a statistical analysis ($P < 0.05$). These variants were subsequently sequenced to confirm the amino acid mutations. Thereinto, 8 samples including C4-B6 (plate number-well position), D5-H2, D5-E2, A2-F1, C5-H8, C1-D4, C5-H4 and C5-H12 (Figure 4b), exhibited amino acid substitution(s) (Table 1) whereas the rest 5 samples were confirmed to be C-r-P^{WT} due to nonsense mutation(s). The eight mutant variants were then subcloned to

defuse mCarmine, generating *C*-terminal His_6-tagged *Is*PETase mutants for enzyme activity determination.

The purified enzyme activity of wild type *Is*PETase and the eight mutant variants were measured using amorphous GfPET film. As results (Figure 5a), 7 out of 8 mutant variants showed 1.3–4.9 folds of improved activity comparing to the wild type enzyme (Table 1), and 6 of which exhibited significant differences according to the one-sided *t*-test analysis. The amino acid (AA) substitution occurred in the 6 activity promoted variants seemed distributed randomly in the three-dimensional structure of *Is*PETase[12] (PDB ID: 5XG0, Figure 5b). With an exception of C4-B6 having 3 AA mutations, the other five mutant variants respectively had a unique AA mutation. The randomly generated mutation sites (Figure 5b) screened from this pilot library will provide new candidates for the iterative mutagenesis and/or mechanism investigations, hopefully generating superior variants based on *Is*PETase or its currently available mutant scaffolds.[16–18]

Feasibility of highly crystallized PET materials for the HTS approach

Highly crystallized PET was reported to be almost inert for *Is*PETase[41] or PET assimilating microorganisms.[42] In addition to amorphous GfPET used for preparation of PET-FDL films, we evaluated the HTS approach by using commercial PET powder LIGHTER™ C98 (Dow, Midland, USA) with a crystallinity of 45.4% determined by differential scanning calorimetry (DSC).

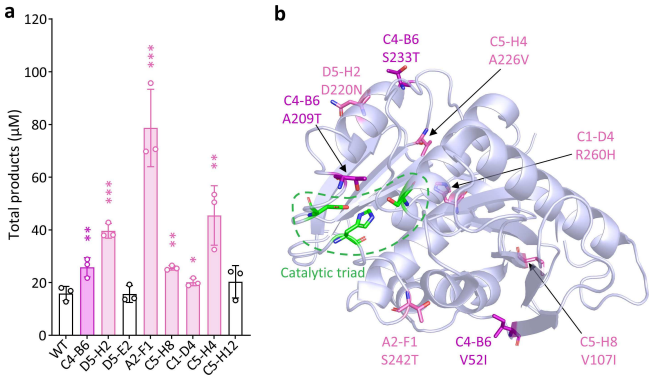

Figure 5. Activity determination of the selected purified mutant variants. a) GfPET film hydrolytic products released by wild type *Is*PETase (WT) and its mutant variants. The reactions were monitored at 40 °C in pH 9.0 glycine–NaOH buffer, incubated for 24 h. The total products including TPA, MHET and BHET of each sample were analyzed by HPLC. Triplicated measurements were conducted for each enzyme. The bars and circles represent the average and individual values of total products concentrations. Statistical analyses using a one-sided *t*-test were performed to compare the product amounts yielded by the variants and WT. Variants with improved activity and statistically significance are indicated as purple (with 3 AA mutations) or pink (with 1 AA mutation) bars. $*P<0.05$, $**P<0.01$, $***P<0.001$. b) Mutation sites distribution in the three-dimensional structure of *Is*PETase (PDB ID: 5XG0).[12] The amino acid substitutions responsible for activity improvement are indicated with purple or pink sticks. The catalytic triad is shown as green sticks within a dashed green circle. Graphic for the three-dimensional structure and site-mutagenesis is generated using the PyMOL program (version 2.5, Schrödinger, http://pymol.sourceforge.net/).

The Z′ factor was determined to be 0.72, also exhibiting an excellent assay. Surprisingly, the average $FI_{494/525}/FI_{603/675}$ value was almost the same level as that of GfPET (124 versus 132) (Figure S7), demonstrating the similar activity of P^{EHA} towards the PET-FDL films derived from amorphous GfPET or high crystallinity PET powder. The crystallinity of PET films was then determined by DSC. As a result, all the solvent cast derived PET films, including those originated from amorphous GfPET and LIGHTER C98, exhibited crystallinity around 30% (Figure S8), which is the same as the previously reported PET film prepared from commercial PET granules.[17] Thus, we suggest that a wide range of PET materials should be suitable for the HTS method. Moreover, according to the fine correlation between $FI_{494/525}$ and total products of PET hydrolysis, the FDL-embedded PET films could also be used as substrates in other contexts for rapid evaluation of PET hydrolysis.

Conclusion

An effective enzyme assay for synthetic polymers is the main challenge for directed evolution of depolymerase due to the insoluble substrate and time-consuming analysis. However, the FDL embedding approach enables quick and sensitive assay for aliphatic polyesters,[27] providing convincing possibilities for application in other kind of polyesters. In this study, by adapting the fluorescein dilaurate (FDL) embedding in PET and in combination with fluorescent protein labelling, we devised and validated a dual fluorescence-based high-throughput screening (HTS) approach for *Is*PETase in 96-well plates. The method is simple and convenient, and the reagents, consumables, and instruments are readily available. Thus, this proof-of-concept work can inspire more HTS assays for those enzymes using insoluble and degradation-resistant polymers as substrates. As the global threat and public concerns growing with plastic wastes accumulation, we envision that further improvement and broader application of this methodology will contribute to the sustainable plastic recycling and value chain innovation.

Owing to decades of research efforts on biodegradation of synthetic plastics, numerous microorganisms and enzymes capable of degrading different kinds of plastics have been identified.[8,43] Thereinto, enzymatic recycling of PET exhibits exciting prospect, not only for PET currently is one of the most recycled plastics in the world, but also because enzymatic approach is harnessed by less value destructive and eco-friendly superiorities.[4] A growing number of directed evolution efforts have unfolded the great potential of catalytic efficiency and thermostability of PET hydrolytic enzymes (PHEs).[16,17,20,21,23,44] The closed-loop recycling of PET by LCC or *Is*PETase variants[19,21] has started to pave an innovative and sustainable path for biological plastic degradation. [45] However, the previous time-consuming and laborious assays restricted the designed mutant library in small scales, thus hindering the exploration of potential interesting variants. The dual fluorescence-based HTS approach for *Is*PETase we established in this study enables rapid screening of thousands of

mutant variants within 4 days, greatly reducing the number of candidates for pure enzyme assays.

In the pilot screening, it is noteworthy that A2-F1 with S242T mutation showed the highest activity rather than C4-B6 —one of the four variants that exhibited relative $FI_{494/525}/FI_{603/675}$ values > 3 during the first-round screening (Figure 4a) and the highest in the second-round screening (Figure 4b). This result indicated that to some extent the fusion of mCarmine to *Is*PETase variants could lead to variation of activity ratios between fused and non-fused enzymes. The ratio changes were also displayed by other mutant variants during the screening and enzymatic assays as listed in Table 1. However, this phenomenon did not cause constraint for the HTS approach, for the success of the screening lay in confining the scope to an acceptable amount of candidates for the enzymatic assays. After two rounds of screening and sequence analysis, the final enzymatic assays successfully generated six significantly improved mutant variants out of eight candidates, exhibiting a highly efficient screening procedure for a large mutant library of PHEs. Finally, given the overall results as briefed in Table 1, a recommended rule for the HTS was deduced: Set a threshold of fold change of 2 for the first-round screening, and conduct triplicated test for the second-round screening and statistical analysis for the significantly elevated variants. Following the principles, we confidently propose that beneficial mutant variants will arise from the enzymatic assays of focused candidates (six improved variants out of eight candidates in this study). Comparing to the recently reported rational designed mutagenesis of different PHEs based on structures,[11,16,20,44] computational redesign and testing,[17] or machine learning aided engineering,[18] this HTS strategy is a promising approach for novel mutant pattern discovery from more ambitious mutagenesis of *Is*PETase or other PHEs.

Experimental Section

Preparation of fluorescent probe (FP) embedded PET films in 96-well microplate

PET-FP films were prepared by following the previously established approach for aliphatic polyesters,[27] with appropriate adaptions and modifications on the solvent and evaporation temperature. Amorphous GfPET films were cut into small pieces and dissolved in HFIP to a final concentration of 20 mg mL^{-1}. Fluorescent probes (FPs), including F, FDA or FDL, were subsequently added to make a series of PET-FP solutions as follows: 5 mg mL^{-1} of PET solutions with 5 μg mL^{-1} of FPs; and 10, 15, or 20 mg mL^{-1} of PET solutions with 5 μg mL^{-1} of FDL. The fluorescent probe embedded PET films were prepared by adding 40 μL per well of PET-FP solutions to black polypropylene 96-well microplate (655209, Greiner, Kremsmünster, Austria), followed by evaporation for 2 h on a HP10 constant temperature heating table (LEBO Science, Jiangyin, China). Consequently, PET-FP films were coated on the bottoms of microplate wells, ready for use as substrates. The resulting PET films with FP proportions (*w*/*w*) were as follows: 1‰ F; 1‰ FDA; 0.25‰, 0.33‰, 0.5‰ and 1‰ FDL.

Binding affinity evaluation of FPs in PET matrix

The spontaneous release of F, FDA and FDL from PET matrix was tested by soaking in 200 μL of glycine–NaOH (pH 9.0) at series of temperatures. The PET-FP films contained 1 μg mg^{-1} of FP in PET. After 48 h of soaking treatment, the buffers were transferred to a new black 96-well plate for fluorescence measurement. The transferred buffers were treated with 50 nM of P^{EHA} for additional 24 h and then fluorescence was recorded again. The fluorescence intensity was detected by a ENSPIE plate reader (Perkin Elmer, Waltham, USA) at the emission wavelength of 525 nm (excitation wavelength: 494 nm). All experiments were performed in triplicate.

Construction of *Is*PETase random mutagenesis library

The *Is*PETase mutation library was constructed based on plasmid pET28a-C-r-P^{WT}. Random mutagenesis of the *Is*PETase encoding region was conducted by error-prone PCR with rTaq DNA polymerase, and the rest of the plasmid backbone was linearized and amplified using the high fidelity PrimeSTAR Max DNA Polymerase. PCR reactions were carried out on a GeneTouch Plus thermocycler (Bioer Technology, Hangzhou, China). The error-prone PCR reactions contained 5 μL of 10×Takara rTaq PCR Buffer (Mg^{2+} free), 5 mM $MgCl_2$, 300 μM $MnSO_4$, 200 μM each of dATP and dGTP, 1 mM each of dCTP and dTTP, 0.2 μM of each primer, 5 ng of template plasmid, and 0.25 μL of Takara rTaq DNA polymerase in a total volume of 50 μL. The thermocycles were as follows: 98 °C for 10 min; 35 cycles of 98 °C for 10 s, 55 °C for 30 s, 72 °C for 1 min; and followed by 5 min at 72 °C. The randomly mutant fragments were inserted into the linearized backbone through seamless cloning using ClonExpress II One Step Cloning Kit. The ligation products were transformed into *E. coli* Rosetta-gami 2(DE3) and spread on LB-Km/Tc plates. The average mutation rate was determined by sequencing 20 samples of randomly selected variants. A library with an average of 1–5 amino acid substitutions per gene (2–9 nucleotide substitutions per gene) were constructed. Single colonies were picked into 96-well deepwell plates and grown overnight at 37 °C in 500 μL LB-Km/Tc media (with 50 μg mL^{-1} of kanamycin and 5 μg mL^{-1} of tetracycline). C-r-P^{WT} expression strains were included in each plate. Afterwards, 500 μL of 40% glycerol was added to each well and the plates were stored at −80 °C as library storage.

Mutant library screening

From the library storage plates, 5 μL of each variants were inoculated to a 96-well deepwell plate containing 200 μL of LB broth containing 50 μg mL^{-1} of kanamycin (Km) and 5 μg mL^{-1} of tetracycline (Tc) (LB-Km/Tc) for overnight preculture. Subsequently, 25 μL each of precultures were inoculated to a new plate containing 400 μL of fresh LB-Km/Tc in each well. After 6 h culture, protein expression was induced by adding isopropyl β-D-1-thiogalactopyranoside (IPTG) to a final concentration of 0.5 mM. Cells were then harvested by centrifugation at 4000×*g* and frozen at −80 °C for at least 2 h before lysing. Cell pellets were lysed by resuspending in 400 μL of lysis buffer (50 mM Na_2HPO_4 buffer, pH 7.4, 10% glycerol, 300 mM NaCl) supplemented with 0.1% Triton-X100, 1 mg mL^{-1} lysozyme, and 2.5 U mL^{-1} DNase I and incubating for 40 min at room temperature. The supernatants containing the crude enzymes were separated from cell debris by centrifugation at 13000×*g* for 60 min. A volume of 200 μL clear cell lysates were transferred into black 96-well microplates for fluorescence detection at the emission wavelength of 675 nm (excitation wavelength: 603 nm). The FDL embedded PET depolymerization was initiated by addition of 10 μL of supernatants from

each well to the PET-FDL coated 96-well plates, to a final volume of 200 μL in 50 mM glycine buffer, pH 9.0. The plates were incubated for 24 h at 40 °C. The green fluorescence intensities of each well were *in situ* monitored at the emission wavelength of 525 nm (excitation wavelength: 494 nm). The $FI_{494/525}/FI_{603/675}$ fluorescence intensity ratios of each well were calculated as the relative activities of the variants. Selected top 50 mutant variants from the above initial screening were inoculated to a new plate for rescreening, which was performed similarly as described above except in a triplicate setup.

In vitro validation of mutant variants

Protein expression and purification procedures were conducted as described in Supporting Information. The amorphous GfPET films were cut into circular form with 6 mm in diameter as substrates. *In vitro* catalytic activity assays with the purified variants were subsequently performed. The GfPET film was soaked in 500 μL of glycine/NaOH buffer (pH 9.0) with 50 nM of *Is*PETase or its mutant variants. The reaction mixture was incubated at 40 °C for 24 h, after which GfPET films were removed from reaction mixture. The enzymes were denatured by heating at 100 °C for 10 min and removed by centrifugation at 14000 × *g* for 10 min, and the supernatants were analyzed by HPLC.

Acknowledgements

This work was supported by the National Key Research and Development Program of China (2019YFA0706900); the National Natural Science Foundation of China (32025001 and 32071266); the Natural Science Foundation of Shandong Province, China (ZR2019ZD20). We thank Professor Rey-ting Guo from Hubei University for kindly providing MHET, and the expression vector plasmids for Is*PETase and* Is*PETase*$^{S121E/D186H/R280A}$*. We also thank Dr. Xi Hu from Quantum Design (Beijing) Co., Ltd, Beijing, China for helping with the O-PTIR analysis.*

Conflict of Interest

The authors declare no conflict of interest.

Data Availability Statement

The data that support the findings of this study are available from the corresponding author upon reasonable request.

Keywords: plastic biodegradation · PET hydrolase · high-throughput screening · fluorogenic probe · directed evolution

[1] H. Millet, P. Vangheluwe, C. Block, A. Sevenster, L. Garcia, R. Antonopoulos in *Issues in Environmental Science and Technology* (Eds.: R. M. Harrison, R. E. Hester), Royal Society of Chemistry, Cambridge, **2018**, pp. 1–20.
[2] a) M. MacLeod, H. P. H. Arp, M. B. Tekman, A. Jahnke, *Science* **2021**, *373*, 61–65; b) R. Geyer, J. R. Jambeck, K. L. Law, *Sci. Adv.* **2017**, *3*, e1700782.
[3] A. M. Brandon, C. S. Criddle, *Curr. Opin. Biotechnol.* **2019**, *57*, 160–166.
[4] L. DeFrancesco, *Nat. Biotechnol.* **2020**, *38*, 665–668.
[5] S. R. Nicholson, N. A. Rorrer, A. C. Carpenter, G. T. Beckham, *Joule* **2021**, *5*, 673–686.
[6] N. George, T. Kurian, *Ind. Eng. Chem. Res.* **2014**, *53*, 14185–14198.
[7] I. Taniguchi, S. Yoshida, K. Hiraga, K. Miyamoto, Y. Kimura, K. Oda, *ACS Catal.* **2019**, *9*, 4089–4105.
[8] C.-C. Chen, L. Dai, L. Ma, R.-T. Guo, *Nat. Chem. Rev.* **2020**, *4*, 114–126.
[9] S. Yoshida, K. Hiraga, T. Takehana, I. Taniguchi, H. Yamaji, Y. Maeda, K. Toyohara, K. Miyamoto, Y. Kimura, K. Oda, *Science* **2016**, *351*, 1196–1199.
[10] H. P. Austin, M. D. Allen, B. S. Donohoe, N. A. Rorrer, F. L. Kearns, R. L. Silveira, B. C. Pollard, G. Dominick, R. Duman, K. El Omari, V. Mykhaylyk, A. Wagner, W. E. Michener, A. Amore, M. S. Skaf, M. F. Crowley, A. W. Thorne, C. W. Johnson, H. L. Woodcock, J. E. McGeehan, G. T. Beckham, *Proc. Natl. Acad. Sci. USA* **2018**, *115*, E4350–E4357.
[11] S. Joo, I. J. Cho, H. Seo, H. F. Son, H.-Y. Sagong, T. J. Shin, S. Y. Choi, S. Y. Lee, K.-J. Kim, *Nat. Commun.* **2018**, *9*, 382.
[12] X. Han, W. Liu, J.-W. Huang, J. Ma, Y. Zheng, T.-P. Ko, L. Xu, Y.-S. Cheng, C.-C. Chen, R.-T. Guo, *Nat. Commun.* **2017**, *8*, 2106.
[13] C.-C. Chen, X. Han, X. Li, P. Jiang, Du Niu, L. Ma, W. Liu, S. Li, Y. Qu, H. Hu, J. Min, Y. Yang, L. Zhang, W. Zeng, J.-W. Huang, L. Dai, R.-T. Guo, *Nat. Catal.* **2021**, *4*, 425–430.
[14] B. Liu, L. He, L. Wang, T. Li, C. Li, H. Liu, Y. Luo, R. Bao, *ChemBioChem* **2018**, *19*, 1471–1475.
[15] Y. Ma, M. D. Yao, B. Z. Li, M. Z. Ding, B. He, S. Chen, X. Zhou, Y. J. Yuan, *Engineering-PRC* **2018**, *4*, 888–893.
[16] H. F. Son, I. J. Cho, S. Joo, H. Seo, H.-Y. Sagong, S. Y. Choi, S. Y. Lee, K.-J. Kim, *ACS Catal.* **2019**, *9*, 3519–3526.
[17] Y. Cui, Y. Chen, X. Liu, S. Dong, Y. Tian, Y. Qiao, R. Mitra, J. Han, C. Li, X. Han, W. Liu, Q. Chen, W. Wei, X. Wang, W. Du, S. Tang, H. Xiang, H. Liu, Y. Liang, K. N. Houk, B. Wu, *ACS Catal.* **2021**, *11*, 1340–1350.
[18] H. Lu, D. J. Diaz, N. J. Czarnecki, C. Zhu, W. Kim, R. Shroff, D. J. Acosta, B. R. Alexander, H. O. Cole, Y. Zhang, N. A. Lynd, A. D. Ellington, H. S. Alper, *Nature* **2022**, *604*, 662–667.
[19] S. Sulaiman, S. Yamato, E. Kanaya, J.-J. Kim, Y. Koga, K. Takano, S. Kanaya, *Appl. Environ. Microbiol.* **2012**, *78*, 1556–1562.
[20] W. Zeng, X. Li, Y. Yang, J. Min, J.-W. Huang, W. Liu, Du Niu, X. Yang, X. Han, L. Zhang, L. Dai, C.-C. Chen, R.-T. Guo, *ACS Catal.* **2022**, *12*, 3033–3040.
[21] V. Tournier, C. M. Topham, A. Gilles, B. David, C. Folgoas, E. Moya-Leclair, E. Kamionka, M.-L. Desrousseaux, H. Texier, S. Gavalda, M. Cot, E. Guémard, M. Dalibey, J. Nomme, G. Cioci, S. Barbe, M. Chateau, I. André, S. Duquesne, A. Marty, *Nature* **2020**, *580*, 216–219.
[22] V. Pirillo, L. Pollegioni, G. Molla, *FEBS J.* **2021**, *288*, 4730–4745.
[23] A. Nakamura, N. Kobayashi, N. Koga, R. Iino, *ACS Catal.* **2021**, *11*, 8550–8564.
[24] U. Markel, K. D. Essani, V. Besirlioglu, J. Schiffels, W. R. Streit, U. Schwaneberg, *Chem. Soc. Rev.* **2020**, *49*, 233–262.
[25] J. B. Grimm, L. M. Heckman, L. D. Lavis, *Prog. Mol. Biol. Transl. Sci.* **2013**, *113*, 1–34.
[26] Y. Qiao, R. Hu, D. Chen, L. Wang, Z. Wang, H. Yu, Y. Fu, C. Li, Z. Dong, Y.-X. Weng, W. Du, *J. Hazard. Mater.* **2021**, *424*, 127417.
[27] M. T. Zumstein, H. E. Kohler, K. McNeill, M. Sander, *Environ. Sci. Technol.* **2017**, *51*, 4358–4367.
[28] C. P. Toseland, *J. Chem. Biol.* **2013**, *6*, 85–95.
[29] Y. Yang, J. Yang, W.-M. Wu, J. Zhao, Y. Song, L. Gao, R. Yang, L. Jiang, *Environ. Sci. Technol.* **2015**, *49*, 12087–12093.
[30] Y. Su, X. Hu, H. Tang, K. Lu, H. Li, S. Liu, B. Xing, R. Ji, *Nat. Nanotechnol.* **2022**, *17*, 76–85.
[31] O. Klementieva, C. Sandt, I. Martinsson, M. Kansiz, G. K. Gouras, F. Borondics, *Adv. Sci.* **2020**, *7*, 1903004.
[32] a) H. Xu, W. Liang, L. Ning, Y. Jiang, W. Yang, C. Wang, F. Qi, L. Ma, L. Du, L. Fourage, Y. J. Zhou, S. Li, *ChemCatChem* **2020**, *12*, 80–84; b) L. Ma, F. Li, X. Zhang, H. Chen, Q. Huang, J. Su, X. Liu, T. Sun, B. Fang, K. Liu, D. Tang, D. Wu, W. Zhang, L. Du, S. Li, *Sci. China. Life. Sci.* **2022**, *65*, 550–560.
[33] W. Zhang, L. Du, Z. Qu, X. Zhang, F. Li, Z. Li, F. Qi, X. Wang, Y. Jiang, P. Men, J. Sun, S. Cao, C. Geng, F. Qi, X. Wan, C. Liu, S. Li, *Proc. Natl. Acad. Sci. USA* **2019**, *116*, 13305–13310.
[34] G. Kovačević, R. Ostafe, A. M. Balaž, R. Fischer, R. Prodanović, *J. Biosci. Bioeng.* **2019**, *127*, 30–37.
[35] A. Fabritius, D. Ng, A. M. Kist, M. Erdogan, R. Portugues, O. Griesbeck, *Cell Chem. Biol.* **2018**, *25*, 1554–1561.e8.
[36] X. Chen, J. L. Zaro, W.-C. Shen, *Adv. Drug Delivery Rev.* **2013**, *65*, 1357–1369.

[37] B. C. Knott, E. Erickson, M. D. Allen, J. E. Gado, R. Graham, F. L. Kearns, I. Pardo, E. Topuzlu, J. J. Anderson, H. P. Austin, G. Dominick, C. W. Johnson, N. A. Rorrer, C. J. Szostkiewicz, V. Copié, C. M. Payne, H. L. Woodcock, B. S. Donohoe, G. T. Beckham, J. E. McGeehan, *Proc. Natl. Acad. Sci. USA* **2020**, *117*, 25476–25485.
[38] a) Z. Liu, Y. Zhang, J. Wu, *Enzyme Microb. Technol.* **2022**, *156*, 110004; b) N. Büscher, G. V. Sayoga, K. Rübsam, F. Jakob, U. Schwaneberg, S. Kara, A. Liese, *Org. Process Res. Dev.* **2019**, *23*, 1852–1859.
[39] M. Z. Lin, M. R. McKeown, H.-L. Ng, T. A. Aguilera, N. C. Shaner, R. E. Campbell, S. R. Adams, L. A. Gross, W. Ma, T. Alber, R. Y. Tsien, *Chem. Biol.* **2009**, *16*, 1169–1179.
[40] J. H. Zhang, T. D. Chung, K. R. Oldenburg, *J. Biomol. Screening* **1999**, *4*, 67–73.
[41] S. Yoshida, K. Hiraga, T. Takehana, I. Taniguchi, H. Yamaji, Y. Maeda, K. Toyohara, K. Miyamoto, Y. Kimura, K. Oda, *Science* **2016**, *353*, 759.
[42] N. E. Wallace, M. C. Adams, A. C. Chafin, D. D. Jones, C. L. Tsui, T. D. Gruber, *Environ. Microbiol. Rep.* **2020**, *12*, 578–582.
[43] J. Ru, Y. Huo, Y. Yang, *Front. Microbiol.* **2020**, *11*, 442
[44] X.-Q. Chen, Z.-Y. Guo, L. Wang, Z.-F. Yan, C.-X. Jin, Q.-S. Huang, D.-M. Kong, D.-M. Rao, J. Wu, *J. Hazard. Mater.* **2022**, *433*, 128816.
[45] P. Liu, T. Zhang, Y. Zheng, Q. Li, T. Su, Q. Qi, *Eng. Microbiol.* **2021**, *1*, 100003..

Manuscript received: November 1, 2022
Revised manuscript received: December 3, 2022
Accepted manuscript online: December 13, 2022
Version of record online: January 9, 2023